CHAPTER 6

APPLICATIONS

This chapter describes the applications of the developed ECDL for the spectroscopy, wavelength stabilization, fine-tuning of a channel-selectable laser, and liquid crystal (LC) cell gap measurements. The scanning spectrum of sub-Doppler resonances of the rubidium D_2-line is demonstrated. The performances of wavelength stabilized to an étalon of the developed and a commercial ECDL's are compared. A channel-selectable ECDL can be frequency fine-tuned by employing an intracavity NLC cell. Finally, a promising application for the LC cell gap measurements is described in detail. Several factors that limit the measurement accuracy are discussed.

6.1 Sub-Doppler resonances of the rubidium D_2-line

6.1.1 Doppler-free saturated spectroscopy

One of the essential advantages that single-mode ECDL can offer for high-resolution spectroscopy is the possibility of overcoming the limitation set by Doppler broadening. Saturation spectroscopy is based on the velocity-selective saturation of Doppler-broadened molecular transitions. Saturated absorption spectroscopy [76] is an important technique in Doppler-free high-resolution spectroscopy of atoms and molecules. The saturated absorption spectrum is used as an absolute frequency reference and/or a frequency discriminator to frequency stabilized lasers [77-83].

The experimental arrangement for doing Doppler-free saturated absorption spectroscopy is shown in Fig. 6.1. Two counter-propagating laser beams derived from a single laser beam are sent through an atomic vapor cell. While the "pump" beam has a high intensity and serves to make a large fraction of the atoms are pumped to the excited state of transition, producing what is called saturation of the transition. The "probe" beam passing through the saturated medium will experience increased transparency, or reduced absorption, due to the reduction in the number of ground state atoms available to absorb the probe beam.

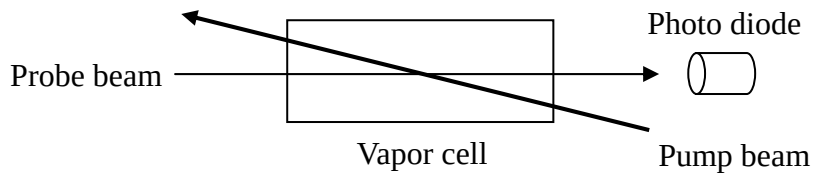

Fig. 6.1 Basic experimental arrangement for saturation spectroscopy

If the pump beam is blocked and only the probe beam goes through the vapor cell, one obtains a simple absorption line exhibiting a strong Doppler broadening. Typically, the Doppler broadening at room temperature exceeds the natural linewidth by two orders of magnitude. Now, if in addition the pump beam is sent through the vapor cell Lamb dip [76] appears in the probe-beam signal at the resonance frequency $\nu=\nu_0$ of the atomic transition. Atoms moving with different speeds along the pump-probe axis absorb laser light of different frequencies because of the Doppler effects. Only for atoms having zero velocity along the long axis of the vapor cell the two counter-propagating laser beams have the same frequency. Atoms at zero velocity, however, do see both the pump and the probe beam. The high intensity of the pump-beam leads to a high absorption rate. If the pump-beam intensity is high enough, the ground state is significantly deplete and therefore the absorbance of the probe beam is reduced compared to the case without pump beam. The width of the Lamb dip is determined by the natural linewidth of the atomic transition and is much narrower than the Doppler width.

6.1.2 Rubidium D_2-line

Natural rubidium (Rb) has two stable isotopes, ^{85}Rb and ^{87}Rb, in proportions of 72.3 % and 27.3 %, respectively. At room temperature (25 °C) it can be safely contained in a standard evacuated glass cell and the saturated vapor pressure is 3×10^{-7} torr, which corresponds to an atomic density of 10^{10} cm^{-3}. This atomic density of 10^{10} cm^{-3} shows very strong absorption in the vicinity of 794.7 nm (D_1-line, $5S_{1/2}$ - $5P_{1/2}$) and 780.0 nm (D_2-line, $5S_{1/2}$ - $5P_{3/2}$). The two isotopes with non-vanishing nuclear spins have magnetic and (electric) quadruple moments associated with them, leading to the so-called hyperfine splitting of the atomic energy levels. The energy level diagram for the D_2-line is shown in Fig. 6.2. The Doppler limited absorption profile of the D_2-line is composed of four distinct resonance features over a 6.5-GHz range. The linear absorption profile and hyperfine structure components of D_2-line for the mixture of Rb isotope are shown as Fig. 6.3 [84].

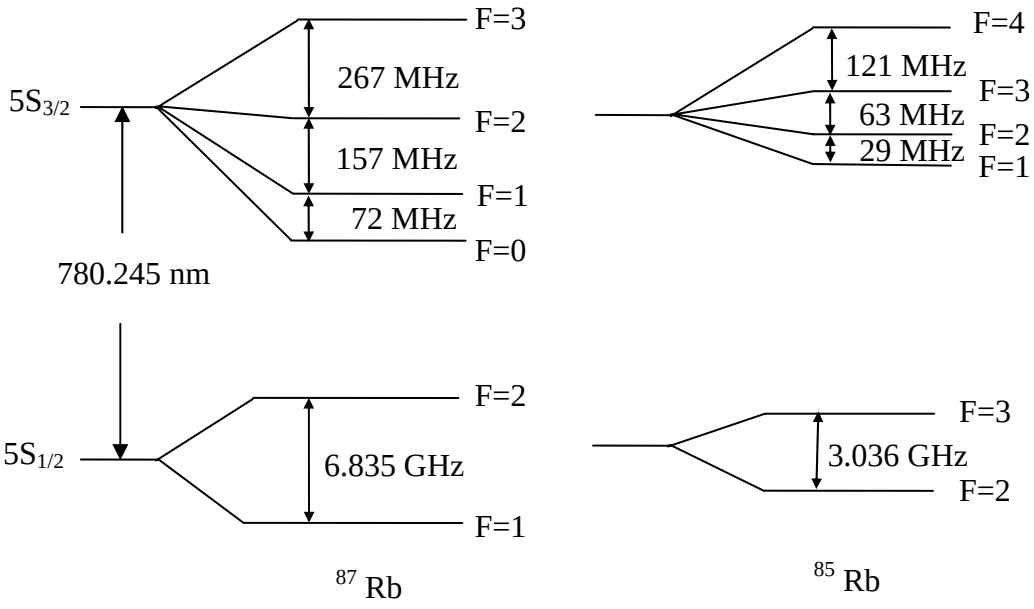

Fig. 6.2 Energy level for the $5S_{1/2}$ to $5S_{3/2}$ transition in ^{85}Rb and ^{87}Rb

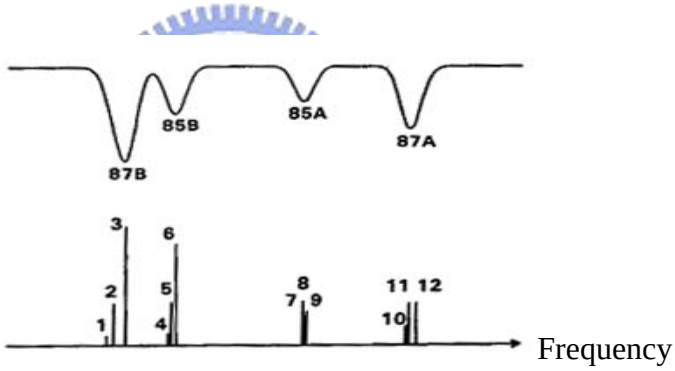

Fig. 6.3 Linear absorption profile and hyperfine structure components of D_2-line for natural Rb [85]

6.1.3 Experimental setup

We use the developed ECDL to observe the sub-Doppler resonances of the rubidium (Rb) atom D_2-line ($5S_{1/2}$ - $5P_{3/2}$, 780 nm). The experimental setup is shown in Fig. 6.4. Laser wavelength of 780.245 nm is tuned by the feedback mirror and measured by a wavelength meter. The output beam from the developed ECDL is split by a beam splitter (BS) into a strong pump beam and a weak probe beam. The strong pump beam passes the Rb cell in clockwise direction. The probe beam passes the cell in counterclockwise direction. When the transmitted probe-beam intensity is measured as a function of laser frequency, the detected

signal shows the Doppler-broadened absorption profiles. The Rb cell is 25.4 mm in diameter and 25.4 mm long. Scanning the applied voltage of the NLC cell scans laser frequency. The scan range is 200 mV with a scan speed of 30 mHz. We observe the saturated absorption spectrum by an oscilloscope. Sub-Doppler resonance of the 85B and 87B are demonstrated in Fig. 6.5. The offset frequency between these two groups is about 1.14 GHz. The experiment results demonstrate that the developed ECDL system can operate in a single-mode and can be used for spectroscopic applications.

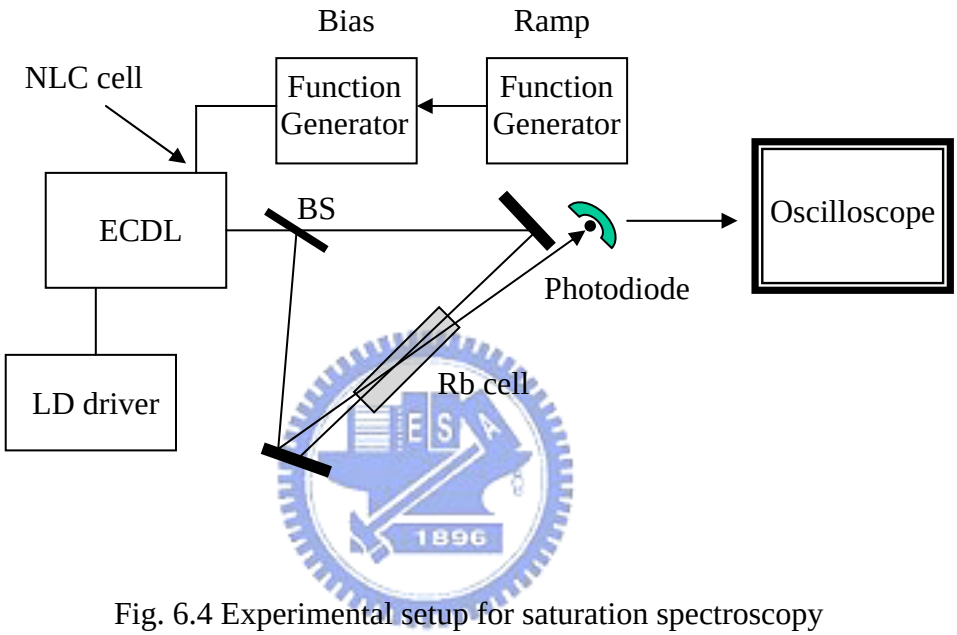

Fig. 6.4 Experimental setup for saturation spectroscopy

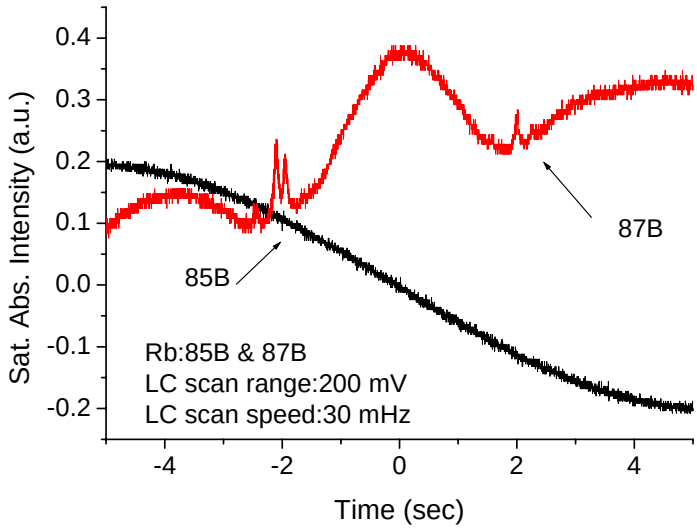

Fig. 6.5 Sub-Doppler resonances of Rb D_2-line

6.2 Wavelength stabilizations

6.2.1 Wavelength locked to an étalon

Though the ECDL's are attractive light sources for many applications, the frequency stability is, however, often poor because of the sensitivity of the cavity to fluctuations in environmental conditions. Numerous studies have been devoted to the frequency stabilization of ECDL's. To reduce the frequency fluctuations, optical feedback phase control is usually employed. An electrical feedback loop to the piezoelectric transducer (PZT) mounted on the grating (Littrow configuration) or the end mirror (Littman-Metcalf configuration) is usually used to adjust the optical feedback phase [85-91]. The electrical feedback signal applied to the electrooptic phase modulators were also demonstrated [92, 93]. In this section, we demonstrate wavelength stabilization of the developed ECDL by feedback controlling the NLC cell.

We use the transmission spectrum of an étalon as the reference to lock the output wavelength of the ECDL. The schematic of locking the ECDL to the étalon is shown in Fig. 6.6. The transmission spectrum of the étalon is used to derive the error signal for a servo loop, which keeps the laser wavelength resonant with the transmission peak. Current modulation and lock-in detection are used to extract the appropriate error signal. The LD is modulated by a 1 kHz sinusoidal wave, which is also the reference signal of the lock-in amplifier. The transmission signal is than demodulated.

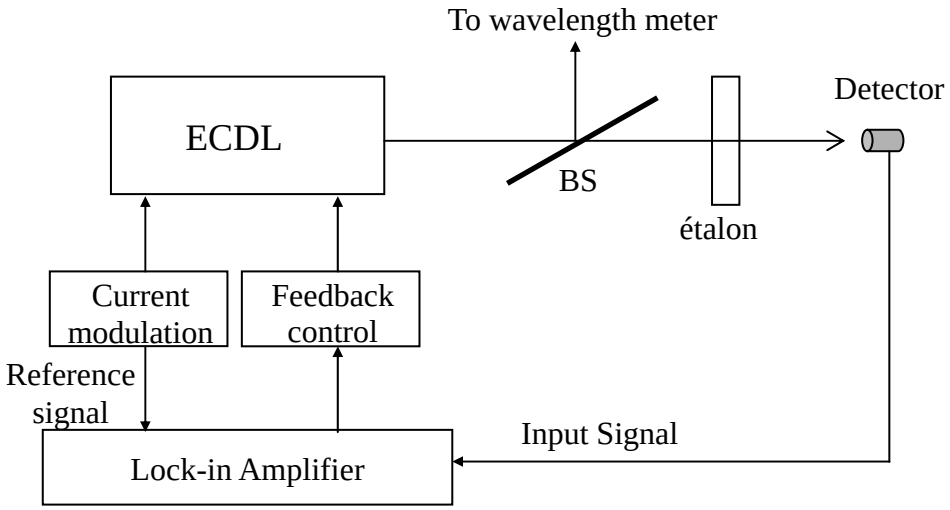

Fig. 6.6 The schematic of locking the ECDL to the transmission peak of an étalon

The traces of scanned transmission spectrum and the first derivative (demodulated) signal are demonstrated in Fig. 6.7. Corrections to the laser cavity length are made by feedback control of the NLC cell. A wavelength meter with resolution of 0.0001 nm monitors the output wavelength.

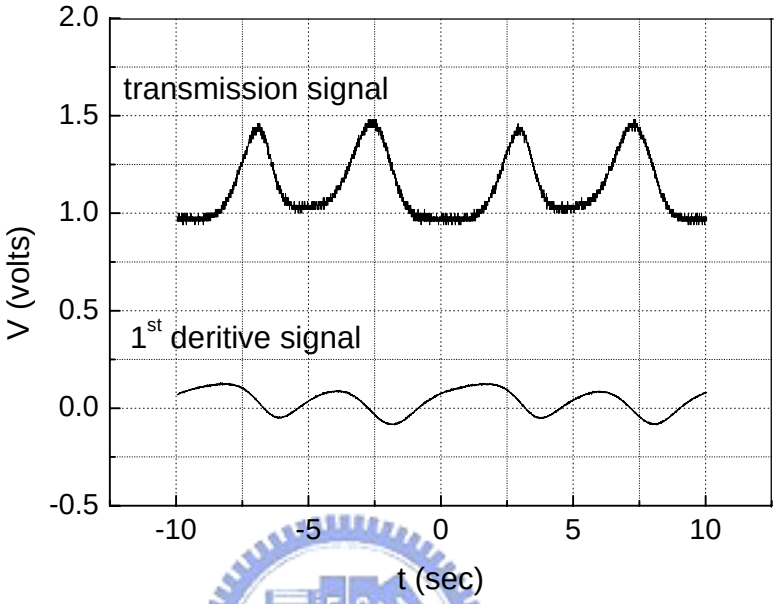

Fig. 6.7 Transmission and 1st derivative spectrum of the étalon

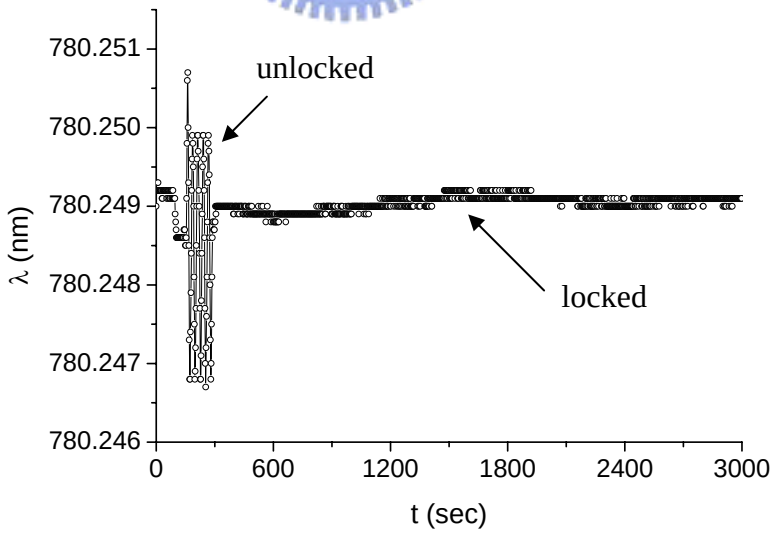

Fig. 6.8 The trace of wavelength fluctuations (unlocked and locked).

The étalon used in the experiment is a 3-mm-thick BK7 glass plate with finesse of 30. The étalon is temperature dependent. Temperature change causes a shift of the wavelength in the

transmission spectrum. In the experiment, we control the environmental temperature at 25 °C ± 0.2 °C. The temperature of the étalon was not controlled. A 50 minutes trace of the wavelength fluctuation of the ECDL when is unlocked and locked is shown in Fig. 6.6. The maximum relative wavelength fluctuation ($\Delta\lambda/\lambda$) of the locked ECDL is 5×10^{-7} for a period of 45 minutes. To consider the temperature coefficient of the étalon, which is $\alpha+n_T$. Where α is the thermal expansion coefficient and $n_T = (dn/dT_{temp})/n$ (n is the refractive index and T_{temp} is the temperature) [94]. The temperature coefficient is 1.2×10^{-5}/°C ($\alpha = 7.4\times10^{-6}$/°C, $n_T = 5\times10^{-6}$/°C) for BK7. The temperature changes about 0.1 °C during the experiment, thus the relative wavelength fluctuation is estimated to be 1.2×10^{-6}.

We stabilize a commercial ECDL (NewFocus model 6313) to the same étalon by feedback control of the PZT. The cavity length of the commercial ECDL is estimated to be ~10 cm. The structure of the ECDL especially the mounting of PZT is important for stable laser output. Here we choose a commercial system instead of the self-established system. The results of the commercial ECDL and of the developed ECDL are compared when both were stabilized. Relative wavelength stabilities expressed by the square root of Allan variance [95] are shown in Fig. 6.9. The calculation of square root of the Allan variance is popular used as a measure of the frequency stability of lasers. The Allan variance is calculated by

$$\sigma_y^{\,2} = \frac{1}{2}\left\langle \left(\Delta \bar{y}^{\tau}\right)^2 \right\rangle = \frac{1}{2(N-1)}\sum_{i=1}^{N-1}\left(f_{i+1}-f_i\right)^2 / f_0^{\,2} \tag{6.1}$$

Where f_i is a signal frequency averaged over the integration time τ, N is the number of averaged frequencies (f_i), and f_0 is the nominal frequency of the laser that is being evaluated. The averaged frequency y_i^{τ} can be obtained by

$$\bar{y}_i^{\tau} = \left(x_{i+1}-x_i\right)/\tau \tag{6.2}$$

Where x_i is the number of frequencies obtained in the time interval τ.

Relative wavelength stabilities of 2.46×10^{-8} (sampling time of 20 s) and 1.49×10^{-8} (sampling time of 60 s) were achieved for feedback control of the NLC cell and feedback control of the PZT, respectively. The stabilities can achieve the same order of magnitude by feedback control of either PZT or NLC cell. The wavelength stability can be further improved by controlling the temperature of the étalon as we mentioned previously, and by additive feedback control of the injection current of the LD [96-98].

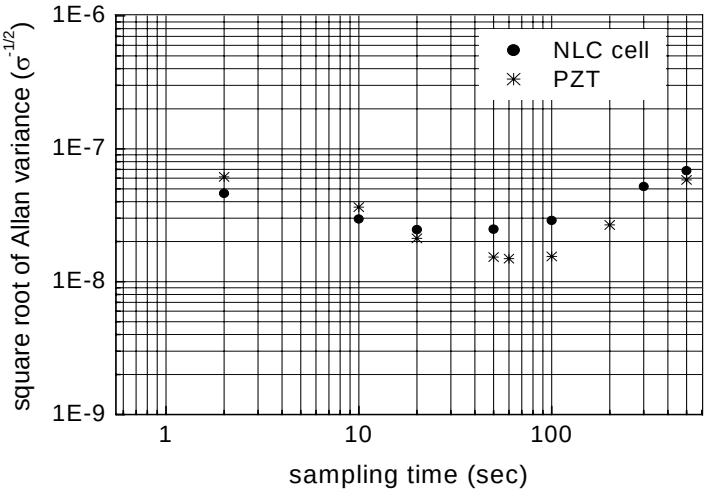

Fig. 6.9 The square root of Allan variance

6.2.2 Frequency locking to femtosecond optical frequency combs

6.2.2.1 Femtosecond optical frequency combs

The output of a mode-locked laser in the time domain consists of a regular train of short pulses separated by time $T=1/f_{rep}$ where f_{rep} is the repetition rate of the laser. In the frequency domain, the output is a comb of frequencies with spacing equal to f_{rep}. If the relative phase of the carrier frequency and the pulse envelope were the same for each pulse in the train, then the comb mode frequencies would be exact integer multiples of the repetition rate. However, this is not generally the case, because the difference between the group and phase velocities inside the laser cavity leads to pulse-to-pulse phase shift $\Delta\phi$ of the carrier with respect to the peak of the pulse envelope. This leads to an offset f_0 of the whole comb from the frequency origin. The spectra of a mode-lock laser in time and frequency domains are shown in Fig. 6.10. The frequency spectrum of a mode-locked laser is therefore a comb with frequencies given by

$$f_m=m\ f_{rep}+f_0 \qquad (6.3)$$

where m is an integer. For Fourier-transform limited pulses, the full width at half maximum of the comb bandwidth is given by the inverse of the pulse duration. Nevertheless, it is desirable to further increase the bandwidth of the comb. Most obviously, this allows larger frequency intervals to be measured. Spectral broadening may be achieved by coupling the output from the mode-locked laser into a short length of microstructure fiber [99]

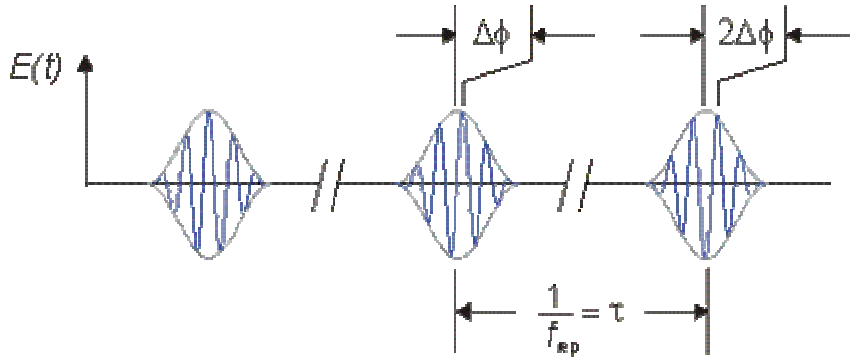

(a)

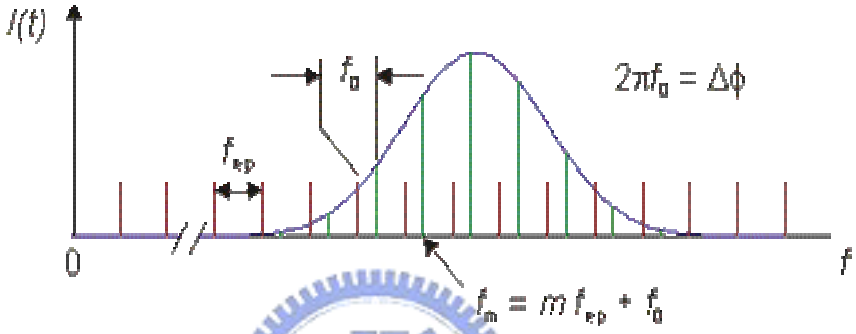

(b)

Fig. 6.10 The spectra of a mode-locked laser in (a) time and (b) frequency domains

6.2.2.2 Frequency locking

The developed ECDL was frequency locked to femtosecond (fs) combs developed by National Measurement Laboratory of Taiwan [100]. The purpose of this experiment is for preliminary study of cw terahertz frequency standards (Chap. 7). We have developed a liquid-crystal-pixel-mirror based ECDL system for generating two wavelengths simultaneously. The gain competition of such dual-wavelengths laser system is quite an issue. To solve this problem, one of the possible ways though hasn't been proved successfully yet is to stabilize the laser frequency. We use the developed ECDL for its simple structure for the preliminary study. Spectral width of the mode-locked fs combs covered from 500 nm to 1180 nm. The repetition rate of the combs is 1 GHz and is locked to a low noise quartz oscillator with short term stabilities of 8×10^{-13} at 1 s. The output beam of the ECDL is arranged to coincide with the beam of the fs combs to generate beat signals.

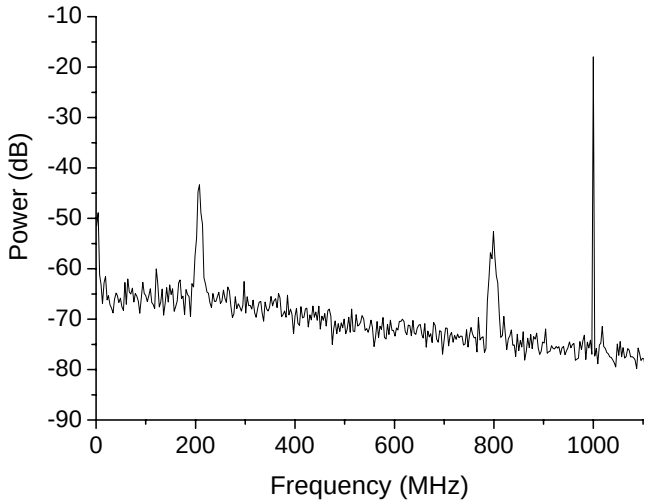

Fig. 6.11 Beat signals of the ECDL and the fs combs

The beat signals detected by an avalanche photodiode are shown in Fig. 6.11. Two beat signals at frequency of 200 MHz and 800 MHz are generated. It is the results of the ECDL beating with adjacent combs. The signal at 1 GHz is the beat signal generated by the fs comb itself. The ECDL was stabilized by feedback control of the NLC cell and the LD current source. In Fig. 6.12, a 10-minutes trace of frequency fluctuations of the beat signal at 800 MHz is plotted. The frequency fluctuation is ~1.5 MHz. This is the preliminary result. For the requirement of high frequency stability, the structure of mounting the NLC cell still has a lot of room for improvement. And to employ a fast feedback loop to the injection current of the LD is also necessary.

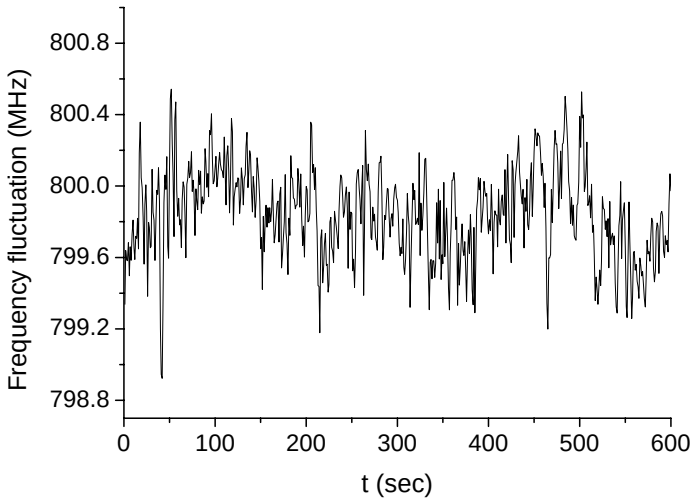

Fig. 6.12 Trace of frequency fluctuations when the ECDL is locked to the fs comb

6.3 Fine-tuning of a digitally channel-selectable laser

The benefits of wavelength tunable/selectable lasers in DWDM (dense wavelength division multiplexed) optical communication systems are widely recognized, e.g., reduction of transmitter inventory and cost-effective standbys in the event of failed channels. For applications such as channel reconfiguration and assignments, the laser wavelength needs to be digitally (discretely) tuned to match the ITU grid. Libatique *et al.* [101] reported a single-longitudinal-mode tunable WDM-channel-selectable fiber laser using a tunable fiber Bragg grating, saturable absorption filter and an intracavity étalon. Alternatively, our group has demonstrated digital tuning of wavelength using liquid crystal pixel mirror (LCPM) at the focal plane of a folded grating-lens cavity in 4-f configuration [63, 64]. In the above designs, however, the laser output could still deviate from the expected wavelength, e.g. the ITU grid, due to environmental fluctuations or mechanical disturbances. For DWDM applications, the required accuracy of the central wavelength of the given channel is ± 5% of the channel spacing. Thus a wavelength fine-tuning mechanism built in the laser is desirable. Conventionally, this can be achieved through temperature control of the LD or mechanical control of the cavity length. A simple approach is to use a LC phase plate in the laser cavity as a fine-tuning element.

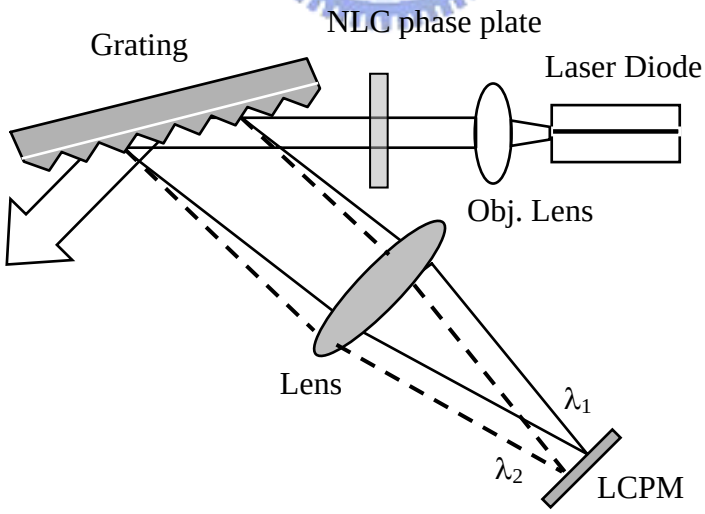

Fig. 6.13 Schematic diagram of the ECDL digitally tuned with the LCPM and fine-tuned with an intracavity NLC phase plate.

The schematic is shown in Fig. 6.13. An ECDL with two LC tuning elements is developed. A planar-aligned NLC cell is applied in our previous design of LCPM based ECDL for which the wavelength can be finely tuned. The LCPM allows digitally tuning of the laser wavelength. Laser wavelength can further be fine-tuned by varying the driving voltages applied to an intracavity NLC phase plate. The results are demonstrated at λ=775 nm. The same concept has be realized for optical communication applications (λ=1.5 um) [102].

The LCPM is based on the design of a normally off-state twisted nematic liquid crystal cell (TNLC) bonded to a polarizer and an Au-coated silicon substrate as the back mirror. The TNLC cell is constructed with a 6-μm-thick NLC (E7 manufactured by Merck) layer sandwiched between indium-tin-oxide (ITO) glass plates. One of the ITO electrodes is patterned. The pattern consists of fifty 100 μm × 2 cm stripes with 5-μm spacing. The NLC phase plate was constructed by sandwiching a 35.5-μm-thick layer of NLC (5CB) layer between two glass plates coated with ITO on the inner surfaces. The output from the AR-coated front facet of a laser diode (Sacher, model 780-40, λ = 775 nm) is collimated by an objective lens (NA=0.47) and directed onto a grazing-incidence diffraction grating (1800 lines/mm) at an angle of 80°. Spectrally selective optical feedback is provided by the retro-reflected first-order-diffracted light from the grating, which is collected by an imaging lens (f=150 cm) and focused on the LCPM. The zeroth-order reflection beam from the grating is the useful output. The cavity length is 60 cm. The cavity mode spacing is 0.25 GHz.

The laser wavelength is digitally tuned and switched by biasing the individual pixels of the LCPM, with wavelength steps $d\lambda$ determined by the center-to-center separation of the adjacent pixel dx (*Eqs*. 4.32)

$$d\lambda = \frac{a\cos\theta_m}{f_{lens}} dx \tag{4.32}$$

where a is the groove spacing of the grating , θ_m is the angle of the first-order diffraction, f_{lens} is the focal length of the imaging lens. For the present laser, the pixel pitch of the LCPM is 105 μm. According to *Eq.* (4.32), the relations of the wavelength variation and the lateral displacement $d\lambda/dx$=3.378 nm/mm. The wavelengths of channels tuned digitally by switching the pixels of the LCPM on and off sequentially are shown in Fig. 6.14.

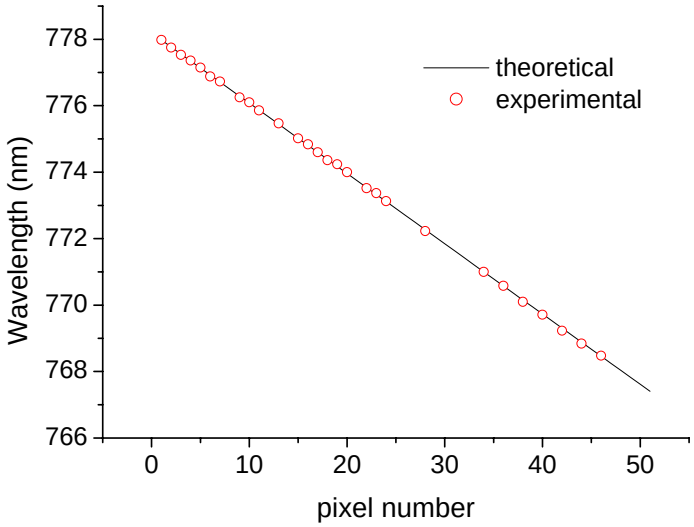

Fig. 6.14 Output wavelength of the ECDL digitally tuned with the LCPM

Output wavelength was digitally tuned to the desired channels by switching on and off the desired pixel of the LCPM. Fine-tuning of the frequency of each channel can be achieved by varying the applied pixel voltages of the LCPM individually. The fine-tuning result of one channel is shown in Fig. 6.15.

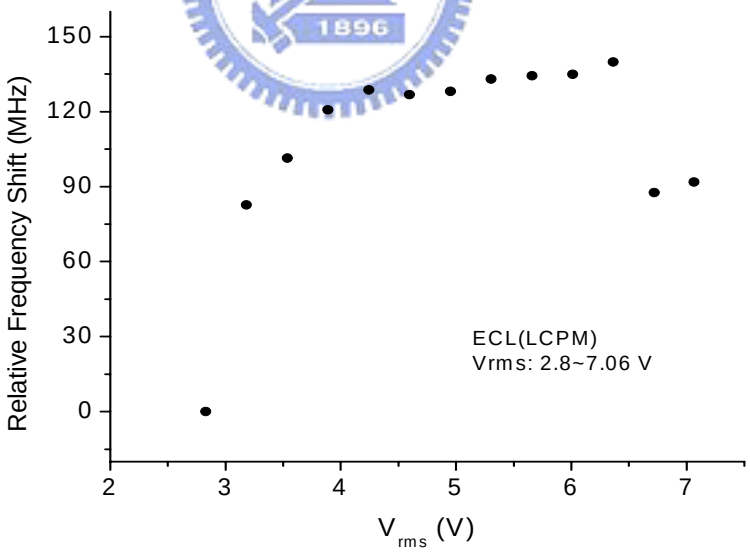

Fig. 6.15 Fine-tuning of one channel by varying the applied pixel voltages of the LCPM

The continuous tuning range is ~140 MHz by tuning the root-mean-square (rms) driving voltage from 2.8 V to 6.36 V. For the voltages larger than 6.36 V mode hop happens. We can see that the frequency shift is not obvious for larger applied voltages. For the voltages larger than 4.24 V the LC pixel is in nearly totally on-state, thus the birefringence of the LC is small

and so is the induced frequency shift. The laser wavelength also can be fine-tuned by varying the voltage driving the NLC cell. According to the previous result of characterizing the 35.5-μm-thick NLC cell, the phase retardation of $\Delta\Phi = 15\pi$ is possible (Fig. 5.2). The tuning range is theoretically to be 3.75 GHz by tuning the driving voltage from 0.4 V to 7.06 V for a 60 cm laser cavity.

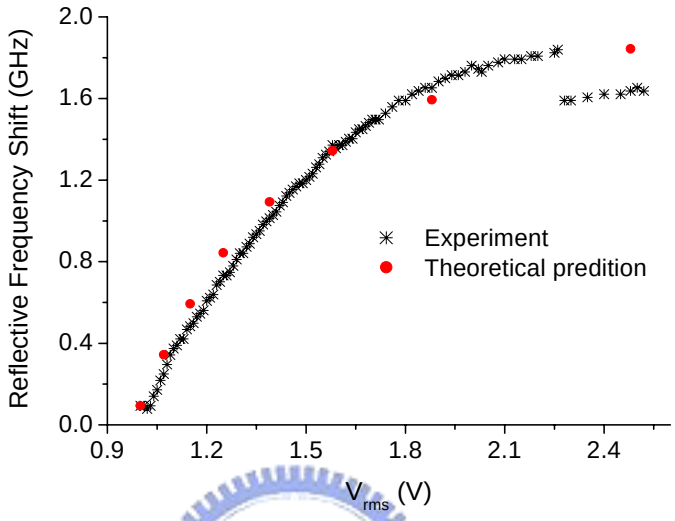

Fig. 6.16 Measured and predicted tuning range of one channel by varying the applied voltages of the NLC cell

A 1.89 GHz range of continuous mode-hop-free wavelength tuning for a given channel is achieved by changing the voltages applied to the NLC phase plate and the bias current of the LD synchronously (Fig. 6.16). Frequency shifts of the laser output as monitored by a scanning Fabry-Perot interferometer (FPI, with Free Spectrum Range, FSR= 2 GHz). The driving voltage increased successively from V_{rms}=0.9 V to 2.52 V. The continuous tuning range achieved is 1.75 GHz from V_{rms}=0.9 V to 2.26 V. The mode-hop-free tuning range is limited by the requirement of dedicated adjustment of the current. The proportionality constant β of the LD is ~6.5 nm/A, which corresponds to 0.0065 nm or 3.25 GHz frequency shift for 1 mA current change. The spacing of the cavity mode is 0.25 GHz, which is equivalent to a 0.08 mA change of LD current. The mode-hop-free tuning range achieved is limited due to manual adjustments of the LD current at present.

6.4 Liquid crystal cell gap measurements

The cell thickness or cell gap is one of the key parameters in the design and fabrication of

liquid crystal displays (LCD). For example, it affects the brightness, contrast ratio and response speed of the LCD's. Traditionally, the cell gaps of an empty [103], or filled [104] LC cell, even LC film with a free surface [105] are measured using interferometric methods. To date, many methods of measuring the cell gap in a filled cell of either transmissive or reflective LCD's have been developed. These include methods based on phase compensation [106-108], Jones Matrix calculation with rotating polarizers [109-110], and spectroscopic [111-115] methods. All of the methods except the interferometric method employ the polarizer and analyzer pairs. The measurement accuracy thus depends on the precision of the rotation stages for the polarizer and analyzer as well as extinction of the pair. By far, the rotating polarizer method is the most popular one. Briefly, the optical transmittance of a LC cell placed between a polarizer and an analyzer is measured as a function of rotation angle. Analysis of the intensity of the transmitted light through the setup provides information on the cell thickness. Small cell gaps, however, can not be easily measured by the rotating polarizer method. To overcome these problems, the total intensity ratio method [111] have been proposed and demonstrated. Cell gap of a reflective twisted nematic LCD was successfully measured by taking the ratio of reflected light intensity at two different polarizer angles [112]. These authors report accuracies of 1~2 %. Measurements by the above two methods are free from multiple solutions for the LC layer thickness, but a suitable range of wavelengths should be chosen to achieve desired accuracy. Chao and Moon [113] proposed a method of determining the cell thickness by the transmission spectrum containing variation points at given polarizer and analyzer angles. The accuracy is primarily limited by the process of choosing a variation point and the error is a little higher than the rotating polarizer method. In this section, we demonstrate another possible application of our ECDL system. The measurement capabilities and accuracy of different methods are summarized in Table 6.1.

A schematic configuration for our LC cell gap (or layer thickness) measurement setup is shown in Fig. 6.17. The LC cell is introduced between the LD and the grating. The output wavelength of the ECDL is measured by a high precision wavelength meter (λ-meter) with a resolution of 0.0001 nm (Burleigh WA-1500). When the planar-aligned LC cell is inside the laser cavity and the laser polarization direction is along its easy direction. Varying the voltage driving the LC cell, its extraordinary index of refraction would change due to field-induced reorientation of the LC director and result in an additional intra-cavity phase retardation $\Delta\Phi$, which corresponds to an optical path difference $\Delta l=\Delta\Phi/k$. The relative wavelength shift of the laser output is then given by

$$\frac{\Delta l}{l} = \frac{\Delta \lambda}{\lambda}; \quad \Delta l = (\Delta n)d \tag{6.4}$$

where l is the cavity length, $\Delta l = (\Delta n)d$ is the variation of the cavity length or the retardation due to the LC, λ is the output wavelength, and Δλ is the corresponding wavelength shift. By measuring the amount of wavelength shift, Δλ, we can calculate the retardation from *Eq*. (6.4). Further, if the birefringence $\Delta n=(n_e-n_o)$ of the LC is known, then the LC cell gap d can be derived.

Table 6.1 Summary of LC cell gap measurement methods

Method	LC material	Cell gap (μm)	Accuracy	Cell type
Interferometric	Empty	5 ~ 10	<1 %	T
Interferometric	ZL13499-100	7.5	<2 %	T
Phase compensation	ZLI-3449-100	1 ~ 15	± 1 %	T
Phase compensation	STN-6238	5, 10, 20	1 %	T
Rotate analyzer and LC cell	5CB	1.20	0.0035 μm	T
Rotate analyzer (Stokes parameter)	E7 K15	25 5	± 0.04 μm	T
Rotate polarizer (TIRM)	ZLI-1559	2.4, 4.2, 7.9	± 0.03 μm	T
Rotate polarizer (Reflected light intensity ratio)	MLC-6815 LCoS	6.44 Δnd=0.192	1.7 % 1.3 %	R
Rotate wave retarder	ZLI-1557	1.8, 2.4, 4.2	± 1 %	R
Crossed polarizer &compensator (Stokes parameter)	E44	10.8	± 0.08 μm	R
Rotate polarizer (TIRM)	ZLI-1557	2.4, 4.2, 6.2	< 1 %	R
Spectroscopic (Differentiating)	ZLI-1557	1.5, 4.2, 6.4	± 0.05 μm	R or T
Spectroscopic ellipsometry (Rotate analyzer and LC cell)	ZLI-5300-100	4.76	1~2 %	T
Rotate analyzer and LC cell	LCoS	Δnd=0.3, 0.5	1 %	R or T
Spectroscopic and single λ (TIRM)	ZLI-2359 ZLI-1557	2.45 6	± 0.03 μm	R
Spectrometer (rotate LC cell)	ZLI-1557	6.2	—	R

T: Transmission, R: Reflective

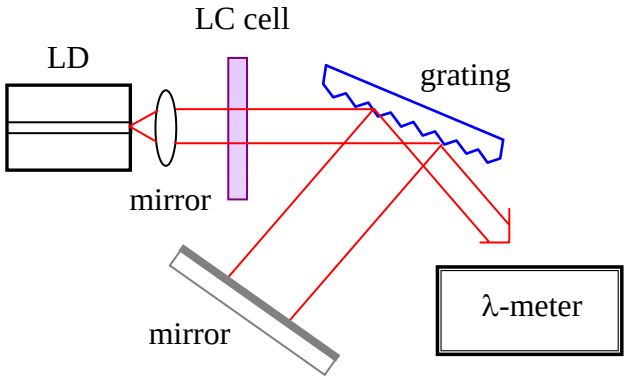

Fig. 6.17 The schematic for transmission type LC cell gap measurement

We prepared two transmission-type planar-aligned nematic LC cells with different cell gaps and LC materials. The empty cells were first measured by using the interferometric method to be 9.6 um and 4.25 um. The LC cells used in the experiment were driven by a sinusoidal wave voltage waveform at 1 kHz and operated at the environmental temperature of 25±0.1 °C. The coefficient for current-tuning of the laser, $\beta=\Delta\lambda/\Delta I$, is 4.7×10^{-3} nm/mA over a range of ± 4 mA around 52 mA. Continuous mode-hop-free tuning of laser wavelength is accomplished by simultaneously changing the voltage driving the LC cell and the bias current of the LD synchronously [116].

6.4.1 LC cell gap of 9.6 μm

One cell of 9.6 μm gap is filled with nematic LC 5CB (Merck) and inserted into the laser cavity. First of all, the cavity length is determined to be 16.62 cm at λ=815.4409 nm by tuning the wavelength while allowing the laser to mode hop. Next, the mode-hop-free tuning range of the laser as a function of the driving voltage of the LC cell is found to be 0.0080 nm (See Fig. 6.18). The synchronous change in LD current required for mode-hop-free tuning is 1.5 mA, which is in good agreement with theoretical prediction of 1.7 mA ($\Delta I=\Delta\lambda/\beta=0.008/4.7\times10^{-3}=1.7$ mA). Thus the retardation due to the LC cell is 1.63 μm according to *Eq.* (6.4). By fitting the data published by S. –T. Wu *et al.* [75], we determine the birefringence of 5CB to be 0.169 at λ =815 nm at T_{temp}=25.1 °C (Appendix A-1). The LC layer thickness d is thus calculated to be 9.65 μm.

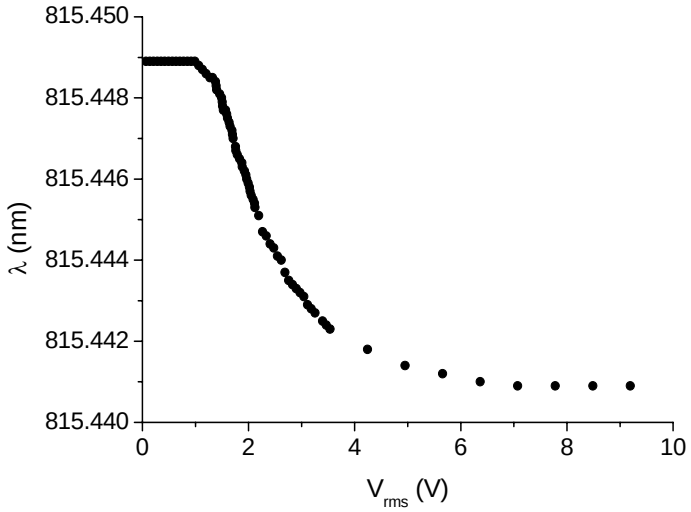

Fig. 6.18 Wavelength shift as a function of the driving voltages (9.6 μm cell)

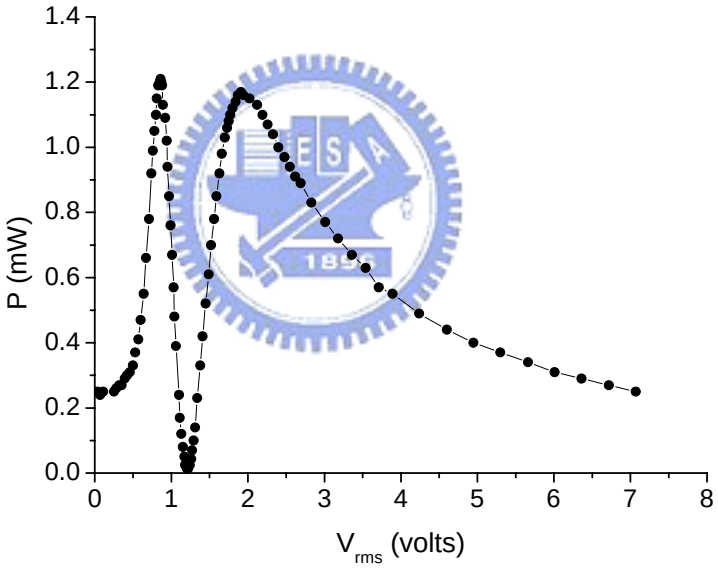

Fig. 6.19 Transmission curve of the 9.6 μm cell measured by the crossed polarizer method

Independently, d is measured by the crossed-polarizer configuration [114]. In this method, the transmittance of the LC cell between crossed polarizers is measured as a function of its driving voltage. The probing laser wavelength is 814.8140 nm. The result is shown in Fig. 6.16. Each cycle in Fig. 6.19 corresponds to a phase retardation of 2π. Thus a phase retardation of $\Delta\Phi=3.73\pi$ is obtained by ramping the driving voltage from 0 V to 10 V. The optical path length of the LC layer is 1.52 μm, corresponding to a thickness of 8.99 μm.

6.4.2 LC cell gap of 4.25 μm

In the second experiment, an empty LC cell of 4.25 μm in thickness is filled with the nematic LC 18523 (BDH), which is a low-birefringence LC that is mixture of highly fluorinated low-refractive-index organic compound additives in hydrocarbon LC hosts. As in the first example, the cavity length is first measured to be 16.62 cm at λ=820.3159 nm. The mode-hop-free tuning range of the laser as a function of the driving voltage of this LC cell is found to be 0.0010 nm (See Fig. 6.20). The corresponding retardation is 0.20 μm. The birefringence of BDH-18523 is determined by interpolating the data from Merck at 0.636 μm and the data published by R. -P. Pan et al. at 1.3 and 1.5 μm [117]. The birefringence is thus estimated to be 0.04737 at λ=820 nm and T=25 °C (Appendix A-2). The LC layer thickness, d is then 4.28 μm. In this case, we can not measure d by using the simple crossed-polarizer configuration. As shown in Fig. 6.21, the transmittance curve is less than one cycle, i.e. the phase retardation ΔΦ is less than 1π.

The LC layer thickness measured by the wavelength tuning method, the interferometric method and the crossed-polarizer method are summarized in Table 6.2. The values listed in the parentheses are the retardations, $d\Delta n$ (unit: μm). LC layer thickness measured by the present method are in good agreements with those measured by the interferometric method, i.e., 1.0 % and 1.2 % for the thick (9.6 μm) and thin (4.25 μm) cells, respectively.

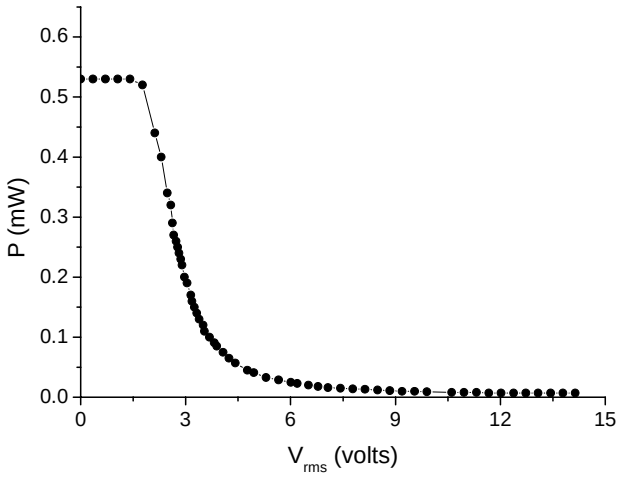

Fig. 6.20 Transmission curve of the 4.25 μm cell measured by the crossed polarizer method

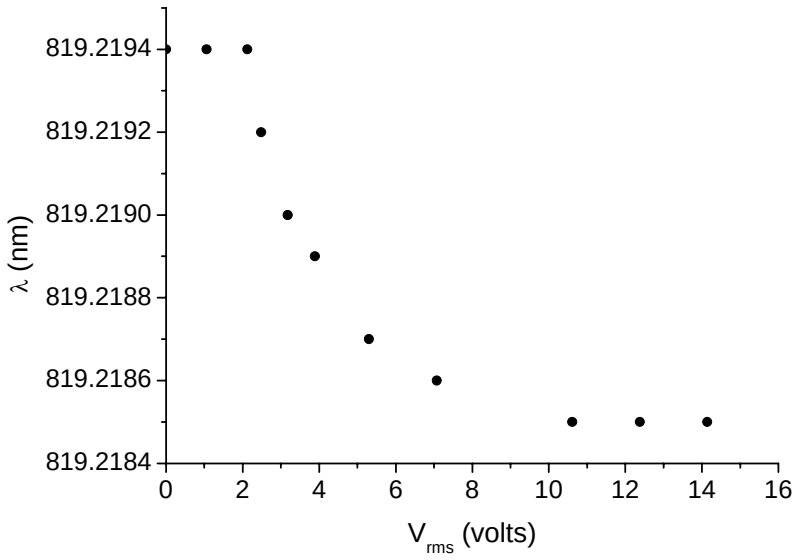

Fig. 6.21 Wavelength shift as a function of the driving voltages (4.25 μm cell)

Table 6.2 Results of LC cell gap measurements

	Interferometric (empty cell)	Mode-hop-free tuning	Transmission measurement
d (μm)	9.6	9.7 (1.63)	9.0 (1.52)
d (μm)	4.25	4.2 (0.20)	

6.4.3 Error analysis

The accuracy of thickness measurements by the present method depends on the uncertainties in the cavity length, birefringence Δn, tilted angle of the LC cell with respect to the propagation direction of the laser, drift of the laser frequency, and the resolution of the wavelength meter. The error sources of the present method are broken down and discussed below:

(1) Wavelength meter：$\delta\lambda$

The resolution of the wavelength meter is 0.0001 nm. The accuracy is assumed to be ±0.00005 nm. The relation between the error of thickness measurement δd and the accuracy of the wavelength meter $\delta(\Delta\lambda)$ can be derived by differentiating *Eq.* (6.4).

$$\delta d \approx \left|\frac{\delta(\Delta\lambda)}{\Delta\lambda}\right| \cdot d \tag{6.5}$$

According to above equation, the measurement error is ±0.06 μm for the cell with d=9.6 μm, for which the wavelength tuning range of the ECDL is Δλ=0.0080 nm, and ±0.21 μm for the cell with d=4.25 μm with the corresponding wavelength tuning range of Δλ=0.0010 nm.

(2) Drift of laser frequency：δf

During environmental perturbation, the frequency of the ECDL in the free-running mode could drift by ~200 MHz during an hour. Thus $\delta f/f=5.43\times10^{-7}$ for λ=815 nm (f=368 THz). The relation between δd and the frequency drift of the free-running mode δf is given by

$$\delta d = \frac{1}{\Delta n}\frac{|\delta f|}{f} \tag{6.6}$$

According to *Eq.* (6.4), the corresponding measurement error is 0.534 μm for a cavity length of 16.62 cm and LC birefringence Δn=0.169 (5CB). For a cell with a thin LC layer, e.g., d=4.25 μm, the measurement time is short (less than 3 minutes). Thus the measurement error due to laser frequency drift is 0.095 μm for $\delta f/f=2.72\times10^{-8}$ and LC birefringence Δn=0.04737 (BDH-18523).

(3) Cavity length： δl

The relation between δd and the accuracy of the measurement of cavity length δl is given by

$$\delta d = |\delta l|\frac{d}{l} \tag{6.7}$$

If the cavity length is known with an accuracy of ± 0.1 mm, and the cavity length is 16.62 cm, the accuracy of the cell gap measurement is ±0.006 μm for the 9.6-μm cell and ±0.003 μm for the 4.25-μm cell.

(4) Birefringence：δ(Δn)

The relations between δd and the accuracy of the birefringence δ(Δn) of the LC can be written as *Eq.* (6.5), and plotted as shown in Fig. 6.22.

$$\delta d = \frac{\Delta\lambda}{\lambda}\ell\frac{\delta(\Delta n)}{(\Delta n)^2} = \frac{d}{\Delta n}\delta(\Delta n) \tag{6.8}$$

The birefringence $\delta(\Delta n)/\Delta T_{temp}$ is -1.524×10^{-3} /°C for 5CB [75]. During the course of the experiment, the room temperature changes by the amount ±0.1 °C. The corresponding variation in birefringence Δn is then 1.524×10^{-4}. The accuracy of the cell gap is thus 0.009 μm for the 9.6-μm cell. The measurement error resulting from variation in Δn is negligible for the 4.25-μm cell.

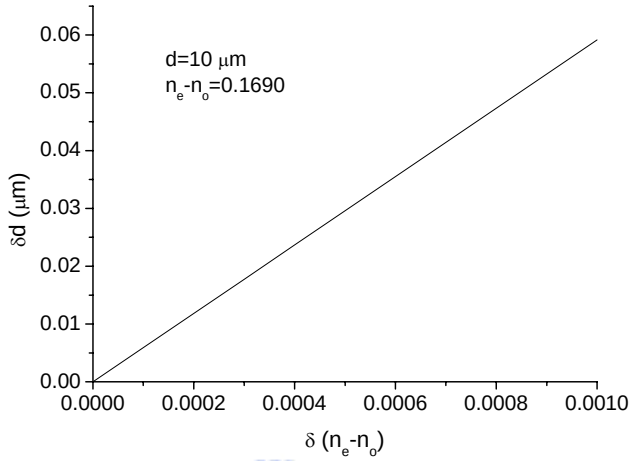

Fig. 6.22 The accuracy of birefringence $\delta(\Delta n)$ versus the accuracy of cell gap δd

(5) Angle： $\delta\theta$

Variation of the angle between the propagation direction of the ECDL and normal of the LC cell θ will also induce measurement errors. The relations between θ, measured thickness d' and the true thickness d is $d'=d/\cos\theta$. The relations between δd and the accuracy of the angle $\delta\theta$ is then

$$\frac{\Delta n \cdot d'}{l} = \frac{\Delta\lambda}{\lambda} \Rightarrow \frac{d}{\cos\theta} = l\frac{\Delta\lambda}{\lambda}\frac{1}{\Delta n} \Rightarrow \delta d = \left| d\tan\theta \cdot \delta\theta \right| \tag{6.9}$$

We plot $\delta\theta$ vs. δd at angles θ from 5° to 30° in Fig. 6.23. The corresponding error in cell gap d is 0.003 μm for a 9.6-μm cell and 0.001 μm for a 4.25-μm cell when the angle θ=10° and $\delta\theta$=0.1° (6 min. of arc).

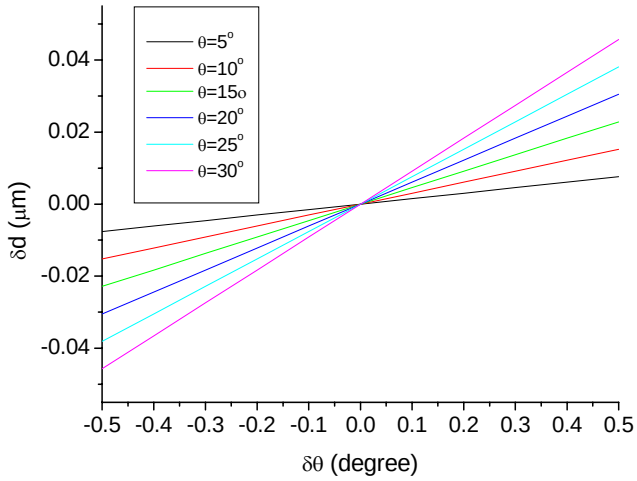

Fig. 6.23 The accuracy of angle $\delta\theta$ versus the accuracy of cell gap δd

The error sources for LC cell gap measurement of the present method are summarized in Table 6.3. Clearly, the accuracy of our cell gap measurement is limited mainly by the resolution of the wavelength meter and the frequency drift of the ECDL. The frequency drift of our ECDL is primarily caused by the thermal drift or mechanical instability of the laser cavity.

Table 6.3 Error sources for LC cell gap measurement

Error sources	Symbols	Quantity	Errors (μm)	
			9.6 μm	4.25 μm
Wavelength meter	$\delta\lambda$	0.00005 nm	0.06	0.21
Drift of laser frequency	δf	200 MHz/hr	0.534	0.095
Cavity length	δl	1 mm	0.006	0.003
Birefringence	$\delta(\Delta n)$	1.524×10^{-4} (ΔT = 0.1 °C)	0.009	—
Angle	$\delta\theta$	0.1° (θ=10°)	0.003	0.001
Combined error			0.537	0.23